ELSEVIER

Brachytherapy ■ (2020) ■

BRACHYTHERAPY

Clinical utility and value contribution of an MRI-positive line marker for image-guided brachytherapy in gynecologic malignancies

Matthew S. Ning[1], Sastry Vedam[2], Jingfei Ma[3], R. Jason Stafford[3], Teresa L. Bruno[1], Mandy Cunningham[1], Christine Starks[1], Ann Lawyer[2], Aradhana M. Venkatesan[4], Li Wang[5], Jihong Wang[2], Nicholas D. Olivieri[1], Alexis B. Guzman[6], James R. Incalcaterra[6], Nikhil G. Thaker[7], Melissa M. Joyner[1], Lilie L. Lin[1], Anuja Jhingran[1], Patricia J. Eifel[1], Ann H. Klopp[1,*]

[1]*Departments of Radiation Oncology, The University of Texas MD Anderson Cancer Center, Houston, TX*
[2]*Departments of Radiation Physics, The University of Texas MD Anderson Cancer Center, Houston, TX*
[3]*Departments of Imaging Physics, The University of Texas MD Anderson Cancer Center, Houston, TX*
[4]*Departments of Diagnostic Radiology, The University of Texas MD Anderson Cancer Center, Houston, TX*
[5]*Departments of Experimental Radiation Oncology, The University of Texas MD Anderson Cancer Center, Houston, TX*
[6]*Departments of Finance, The University of Texas MD Anderson Cancer Center, Houston, TX*
[7]*Department of Radiation Oncology, Arizona Oncology, The US Oncology Network, Tucson, AZ*

ABSTRACT

PURPOSE: The purpose of this study was to investigate the utility of a novel MRI-positive line marker, composed of C4:S (cobalt chloride−based contrast agent) encapsulated in high-density polyethylene tubing, in permitting dosimetry and treatment planning directly on MRI.

METHODS AND MATERIALS: We evaluated the clinical feasibility of the C4:S line markers in nine sequential brachytherapy procedures for gynecologic malignancies, including six tandem-and-ovoid and three interstitial cases. We then quantified the internal resource utilization of an intraoperative MRI-guided procedural episode via time-driven activity-based costing, identifying opportunities for cost-containment with use of the C4:S line markers.

RESULTS: The C4:S line markers demonstrated the strongest positive signal visibility on 3D constructive interference in steady state (CISS)/FIESTA-C followed by T1-weighted sequences, permitting accurate delineation of the applicator lumen and thus the source path. These images may be fused along with traditional T2-weighted sequences for optimal tumor and anatomy contouring, followed by treatment planning directly on MRI. By eliminating postoperative CT for fusion and applicator registration from the procedural episode, use of the C4:S line markers could decrease workflow time and lower total delivery costs per procedure.

CONCLUSIONS: This analysis supports the clinical utility and value contribution of the C4:S line markers, which permit accurate MRI-based dosimetry and treatment planning, thereby eliminating the need for postoperative CT for fusion and applicator registration.

Keywords: MRI-guided; HDR brachytherapy; TDABC; Health care value; Cervical cancer; Endometrial cancer; Positive-contrast marker

Received 28 June 2019; received in revised form 29 November 2019; accepted 30 December 2019.

Financial disclosure: Jingfei Ma is a consultant of C4 Imaging and an inventor of several United States Patents that are licensed to Siemens Healthineers and GE Healthcare. The other authors report no proprietary or commercial conflicts of interest with respect to any product mentioned or concept discussed in this article. This work was supported by the National Cancer Institute, National Institutes of Health, United States to the University of Texas MD Anderson Cancer Center [CA016672].

* Corresponding author. Department of Radiation Oncology, Unit 1422, The University of Texas MD Anderson Cancer Center, 1400 Pressler Street, Houston, TX 77030-4008. Tel.: +1 713 563 2300; fax: +1 713 563 2366.

E-mail address: aklopp@mdanderson.org (A.H. Klopp).

1538-4721/$ - see front matter
https://doi.org/10.1016/j.brachy.2019.12.005

Introduction

Brachytherapy entails the placement of an applicator device as close to the tumor as possible, typically under general anesthesia (1), and is a critical component of radiotherapy for prostate and locally advanced gynecologic malignancies. For high-dose-rate (HDR) brachytherapy, a remote afterloading system transports an encapsulated radioisotopic source through this applicator device to deliver high and conformal target doses over a short time interval (2). Radiation dose calculations are dependent on dwell time and source position in brachytherapy; thus, errors in applicator positioning or source localization will negatively impact dose delivery and the therapeutic ratio of brachytherapy treatment (3–8).

Postoperative axial imaging may be used to optimize the dose distribution during treatment planning, with the aim of elevating target doses and minimizing normal tissue toxicity (9–13). Within the last several years, brachytherapy has progressed toward robust image guidance and in particular MRI-based treatment planning. MRI is preferred over CT for target definition because of the MRI's superiority in soft-tissue contrast (particularly for paracervical soft-tissue extension) (14–20), tumor volume delineation (21–25), and interobserver variability (26). Consistent with these findings, MRI has been regarded as the gold standard imaging modality for interventional procedures (3,27,28) such as image-guided brachytherapy, especially for prostate and gynecologic malignancies (17,21,25,29,30). There has also been growing evidence for improved survival and toxicity outcomes particularly for MRI-guided brachytherapy of gynecologic malignancies (10,13,28,31–35).

Although MRI provides better target volume delineation (25,26,34), the actual localization of the brachytherapy applicator and radiation source on MRI remains a challenge (3–8,29,34,36) because MRI does not directly delineate the applicator lumen and source path (29,37–40). Incorrect catheter reconstruction and mislabeled catheters are two major sources of inaccuracy in HDR brachytherapy (3–8); thus, despite its inferior soft-tissue contrast, CT (with applicator dummy markers) is often still used in addition to MRI for fusion and manual reconstruction of the source path in image-guided brachytherapy (2,29,34,36,41). To remove such redundancy, positive-contrast MRI markers could improve dosimetric precision by facilitating accurate reconstruction directly on MRI (29,37–40). Direct MRI-based dosimetry could also improve quality assurance in multi-institutional protocols through standardization.

Cobalt-chloride complex contrast (C4) agent is an MRI-positive signal agent and has demonstrated utility as a seed marker for low-dose-rate (LDR) prostate brachytherapy (38). In this study, we investigated the utility of a novel MRI-positive brachytherapy "line marker" (Orion MRI-Marker by C4 Imaging, Houston, TX), consisting of C4 complexed with saline (C4:S) and encased within high-density polyethylene (HDPE) tubing. We evaluated the clinical feasibility of these C4:S line markers *in vivo* during nine MRI-guided brachytherapy cases for patients with gynecologic malignancies. After demonstrating signal visibility and the ability to plan directly on MRI, we apply time-driven activity-based costing (TDABC), a bottom-up cost-accounting methodology, to quantify the potential internal cost benefits associated with using these novel MRI-positive line markers.

Methods and materials

Clinical practice and test cases

At our institution, patients who undergo definitive radiation therapy for gynecologic malignancies typically receive pulsed-dose-rate brachytherapy after 5 weeks of external beam radiation therapy with concurrent chemotherapy. Six tandem-and-ovoid (T&O) and three interstitial procedures were included in this series, including three inoperable endometrial and six cervical cancer cases. Four T&O patients received postprocedural MRI after applicator insertion, whereas five underwent applicator insertion under intraoperative MRI guidance to assist with treatment planning. No individually identifiable clinical, demographic, or otherwise protected health information was recorded, analyzed, or reported here for the purposes of this study.

The intraoperative MRI workflow is summarized as follows: general induction is achieved; examination under anesthesia is performed; and sterile preparations are all initiated within the MRI suite. The applicator is then inserted using ultrasound guidance to verify tandem placement within the uterus. After placement, 3D anatomical MRI sequences of the pelvis (including T2-weighted images) are evaluated to ensure appropriate positioning within the uterus and cervix and guide treatment planning.

The patient is subsequently transferred to the postanesthesia care unit for recovery, before CT simulation for manual reconstruction, dosimetric planning (Oncentra planning system, Elekta, Stockholm, Sweden), and treatment delivery via Iridium-192 Nucletron HDR unit (Nucletron, an Elekta company, Elekta AB, Stockholm, Sweden). For the T&O cases, a custom-designed Fletcher-style CT/MR-compatible applicator made of nonferrous plastic material was used, whereas the Venezia Advanced Gynecological Applicator (Elekta, Stockholm, Sweden) was used for our interstitial cases.

Line markers

The Orion line markers are 510(k) cleared by the U.S. Food and Drug Administration, commercially available, used safely in clinical practice, and thus nonexperimental and noninvestigational in nature. Unlike other user-dependent alternatives, these markers are reliably manufactured with support of a fully audited quality assurance

system, ensuring consistent tube stock as well as a consistent method of forming and sealing the marker tip to eliminate variability with respect to distal tube wall thickness and inadvertent air bubble insertion (which can result in multi-millimeter distortions of the distal portion of the catheter). With respect to postinsertion locking mechanism, a rubber stopper design is used at the proximal end to secure the C4 marker after insertion. The C4 markers can be designed for specific lengths, and further work is underway toward an improved, robust locking mechanism that can accommodate different lengths and applicator sizes with varying offsets.

Postimplant MRI sequences

Three cases were imaged on a 1.5-T MRI system, whereas six were imaged on a 3.0-T scanner. Among several differences, 3T in general offers the benefit of increased signal-to-noise ratio (SNR) (42) and allows faster image acquisition (43) as compared to 1.5-T MRI. Three C4:S line markers were used for each T&O case: two inserted into the ovoids and one within the tandem, inserted distally up to the tip, secured with rubber-stopper locking mechanism. In addition to these 3, interstitial cases required additional markers corresponding to number of interstitial catheters used. With the applicator in place, 2D orthogonal plane and 3D anatomical imaging (including T1- and T2-weighted sequences) of the pelvis were assessed without intravenous contrast.

In addition to these standard images, a 3D constructive interference in steady state (CISS) [Siemens]—or analogous fast imaging using steady-state acquisition (FIESTA-C) [GE]—sequence was obtained for each case (44). These imaging protocols used fully refocused gradient-echo pulse technique. Image contrast in FIESTA-C/CISS is dependent on the T2:T1 ratio of the tissue (45); therefore, tissues with both short T1 and long T2 relaxation times (high T2/T1 ratio), such as blood and fat, have high signal on FIESTA-C/CISS (45,46). Advantages of the steady-state imaging include rapid acquisition, excellent SNR, and high isotropic spatial resolution when used in 3D mode (45,47). Clinically, FIESTA-C/CISS is already frequently applied for abdominal imaging, central nervous system pathologies, and surgical planning, with excellent visualization for these indications and sites (48). These optimized sequences add a minimal amount of table time (4:30 min), with 120 slices at 2-mm slice thickness (interpolated to 1-mm).

Both 3D-CISS/Fiesta and 3D-T2 are acquired at 1-mm isotropic resolution. Because both sequences are spin-echo based and use very high receiver bandwidth and the region of interest is close to the center of the magnet (iso-center), the expected geometric distortion from the gradient nonlinearity or B0 inhomogeneity is considered to be insignificant. The uncertainty in fusion of the two images should thus be within the sub-millimeter range, unless there is gross patient motion between the two series (which is uncommon under general anesthesia). Regarding general MR-scanner daily quality assurance (with phantom), a geometric accuracy of +0.5 mm (distance-to-agreement) at 20 cm is targeted, with regular system calibration to avoid geometric distance errors >1 mm.

Time-driven activity-based costing

TDABC analysis consists of several steps, including (1) outlining a step-by-step process map of the episode of care; (2) identifying all resources that are used with each process map step; (3) measuring the actual time contribution for each step by each resource; (4) calculating the capacity cost rate, or cost per minute, of each resource; and (5) aggregating the cost of care delivery throughout the entire process by multiplying the respective capacity cost rate with the time attributed to every resource for each step (49–53). Total cost of a care delivery episode was defined as the summation cost for all resources used for treatment delivery. All costs are based on data from the 2016 fiscal year. For this analysis, a care episode was limited to a single T&O procedure under intraoperative MRI guidance: starting at check-in, followed by anesthesia, continuing through MRI and dosimetry, and culminating with treatment delivery and discharge (without inclusion of followup).

Comprehensive lists of personnel, equipment, and supplies involved at each step were accounted for along with time contributions through direct workflow observation. For personnel time contribution, compensation data were pulled from the PeopleSoft (Oracle Inc., Redwood Shores, CA) payroll application and included salary, bonuses, fringe benefits, support, training, travel, and insurance expenses, approximated through a multiplying factor specific to our institution. Regarding supplies, financial master lists detailing the base cost for each piece of equipment were used to identify the cost of each resource. These costs incorporated purchase price, lifespan (e.g., 7 years), depreciation, and maintenance, guided by institutional and manufacturer recommendations when applicable. This analysis did not include cost of the C4:S markers, which themselves would be associated with some market or wholesale expense to the provider. Indirect facility and overhead costs were approximated and embedded through a multiplying factor specific to our center.

Results

Signal intensity and visibility of C4:S line markers on MRI

C4:S encapsulated in HDPE tubing was visible as a positive line marker on T1-/T2-weighted images and 3D-CISS/FIESTA-C sequences, acquired on either 1.5-T or 3.0-T MRI scanner (although with higher SNR on the 3T scanner as expected). The markers demonstrated their strongest signal on the 3D-CISS/FIESTA-C images (followed next by T1-

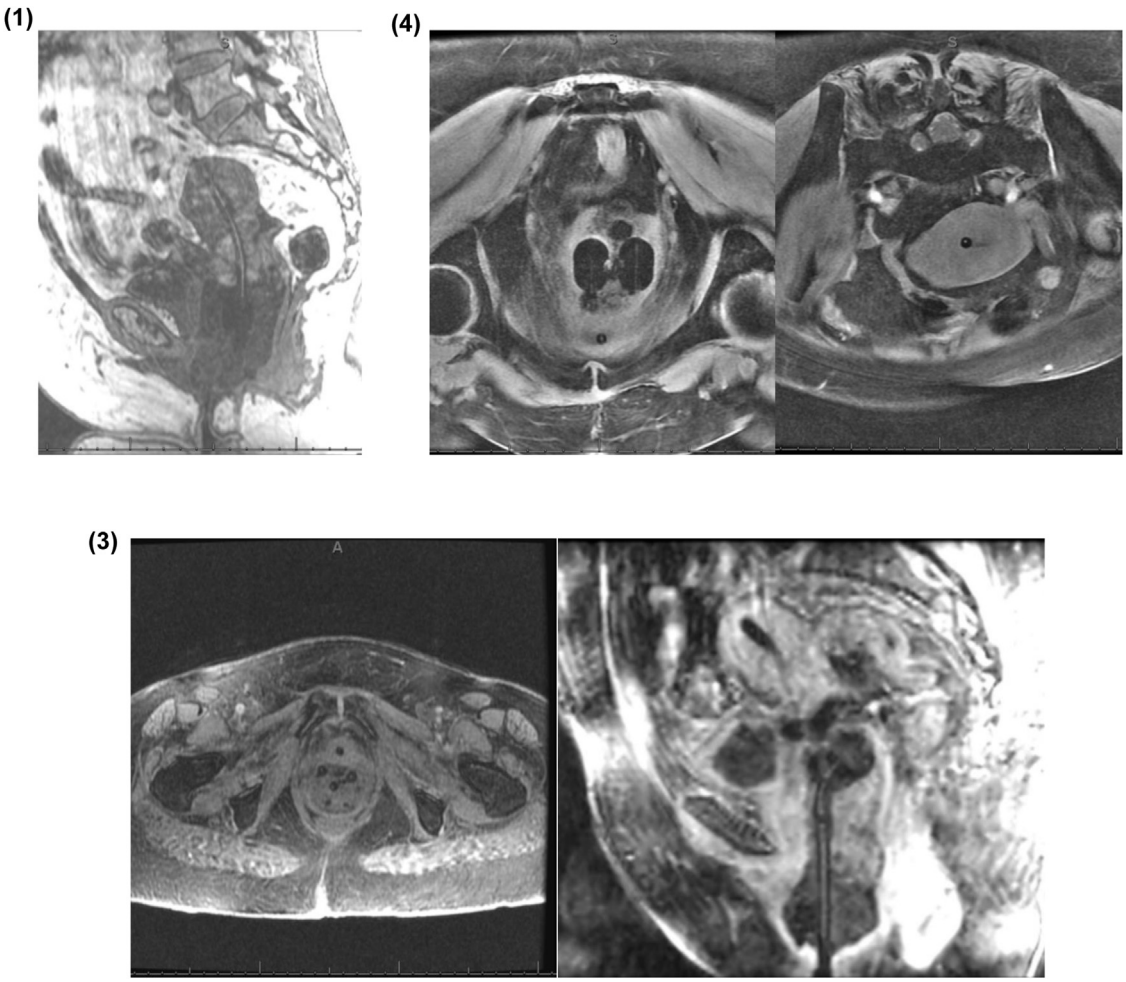

Fig. 1. Example T1-weighted MRI images demonstrating visibility of the C4:S line markers within the gynecologic brachytherapy applicators: on 1.5-T (cases 1 and 3) and 3.0-T (case 4). Labeled by case number.

weighted sequences), permitting accurate delineation of the applicator lumen and thus the source path (Figs. 1–3). This visibility was unaffected by image orientation.

Although C4:S signal was apparent on T2-weighted images, visibility was sometimes lost at the distal tandem and/or ovoid tips, thus posing difficulties with manual source path reconstruction on T2 alone. However, the 3D-CISS/FIESTA-C images were easily fused with traditional T2 images for optimal tumor and anatomy visibility, followed by treatment planning directly on MRI (without need for a separate CT scan). Thus, the 3D-CISS/FIESTA-C protocol may supplement conventional T2-weighted sequences necessary for contouring (48).

Treatment planning dosimetry with C4:S line markers

Given the pilot nature of this feasibility assessment, post-MRI CT scans for fusion and manual reconstruction were obtained as per our standard institutional workflow and back-up measure for the initial four cases. Among these first several cases, plans were developed using both the CT and MR imaging for applicator source modeling, demonstrating their relative agreement and consistency before full implementation. However, our certified medical dosimetrists were able to plan directly on postimplant MRI in all cases, as desired (Fig. 4), through use of the MRI-positive C4:S line markers. Provider confidence increased with sequential case experience; and ultimately, post-MRI CT simulation was excluded for the fifth and subsequent cases.

Cost-shifting through resource consolidation with C4:S line markers

Figures 5a and 5b shows the relative contribution of each resource to the aggregated cost for intraoperative MRI-guided brachytherapy: (*1*) as previously described (53), with incorporation of the additional 3D-CISS/FIESTA-C MRI sequences; and (*2*) after incorporation of the line markers. Our traditional institutional workflow incorporated post-MRI CT scan with applicator dummy markers to allow manual reconstruction of catheter source paths; however, this postoperative CT simulation (and required radiation therapist effort) together accounted for 4% of total

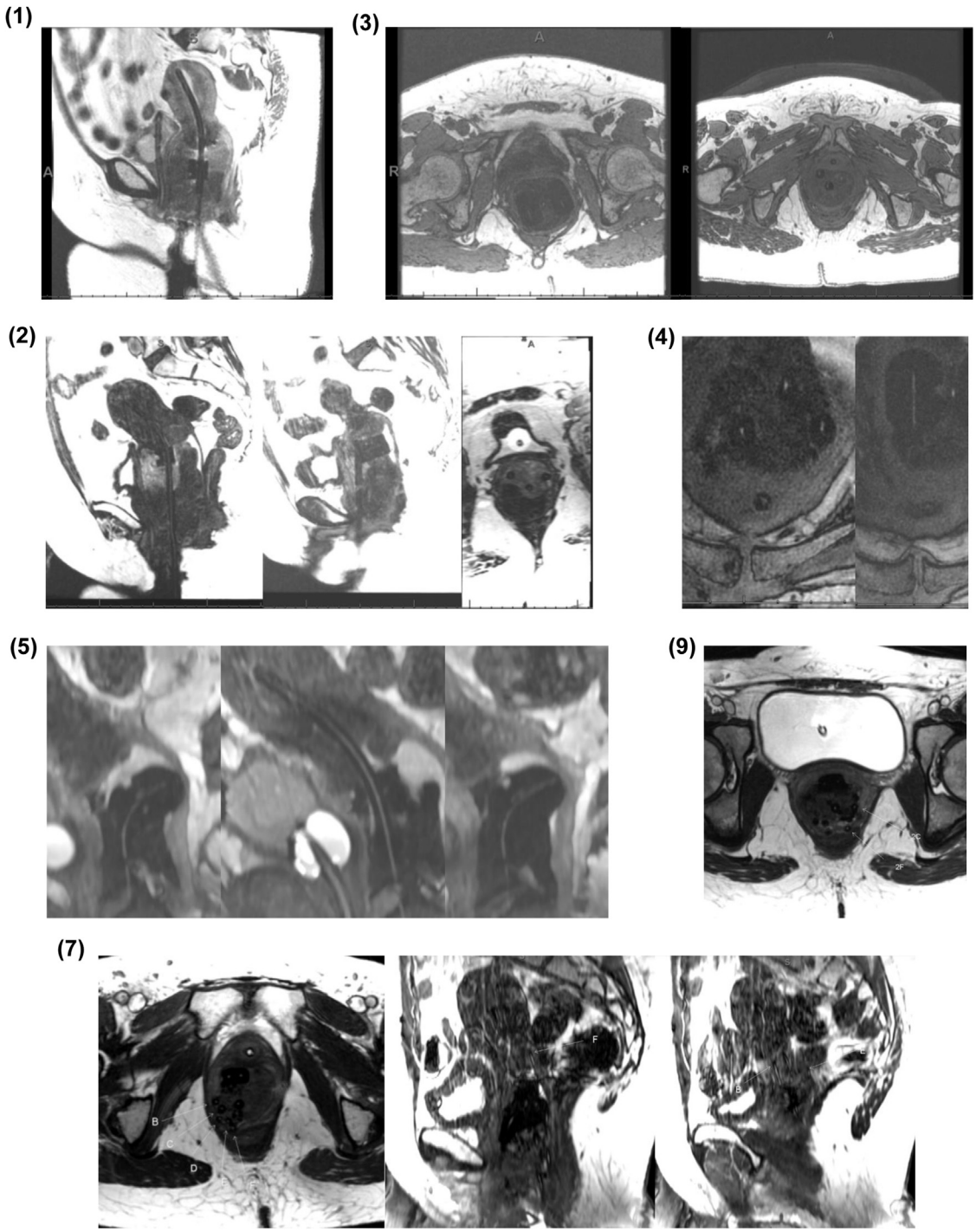

Fig. 2. Example 3D-CISS/FIESTA-C MRI images demonstrating visibility of the C4:S line markers within the gynecologic brachytherapy applicators: on 1.5-T (cases 1−3) and 3.0-T (cases 4−5, 7, 9). Labeled by case number. White arrows label catheter positions for interstitial cases (7 and 9).

costs within the intraoperative MRI-guided workflow (Fig. 5a) (53). By permitting exclusion of this CT scan for fusion and manual reconstruction, the MRI-positive C4:S line markers can result in provider cost savings associated with MRI-guided brachytherapy. Furthermore, use of these markers improves overall process time by eliminating roughly 60 min associated with the CT (and associated patient transport) workflow steps, permitting greater throughput, and potentially freeing up these resources for other uses. By contrast, the additional table time (4:30 min) associated with the 3D-CISS/FIESTA-C sequences were associated with a resource utilization increase of 2, resulting in a net decrease in provider delivery costs associated with marker utilization.

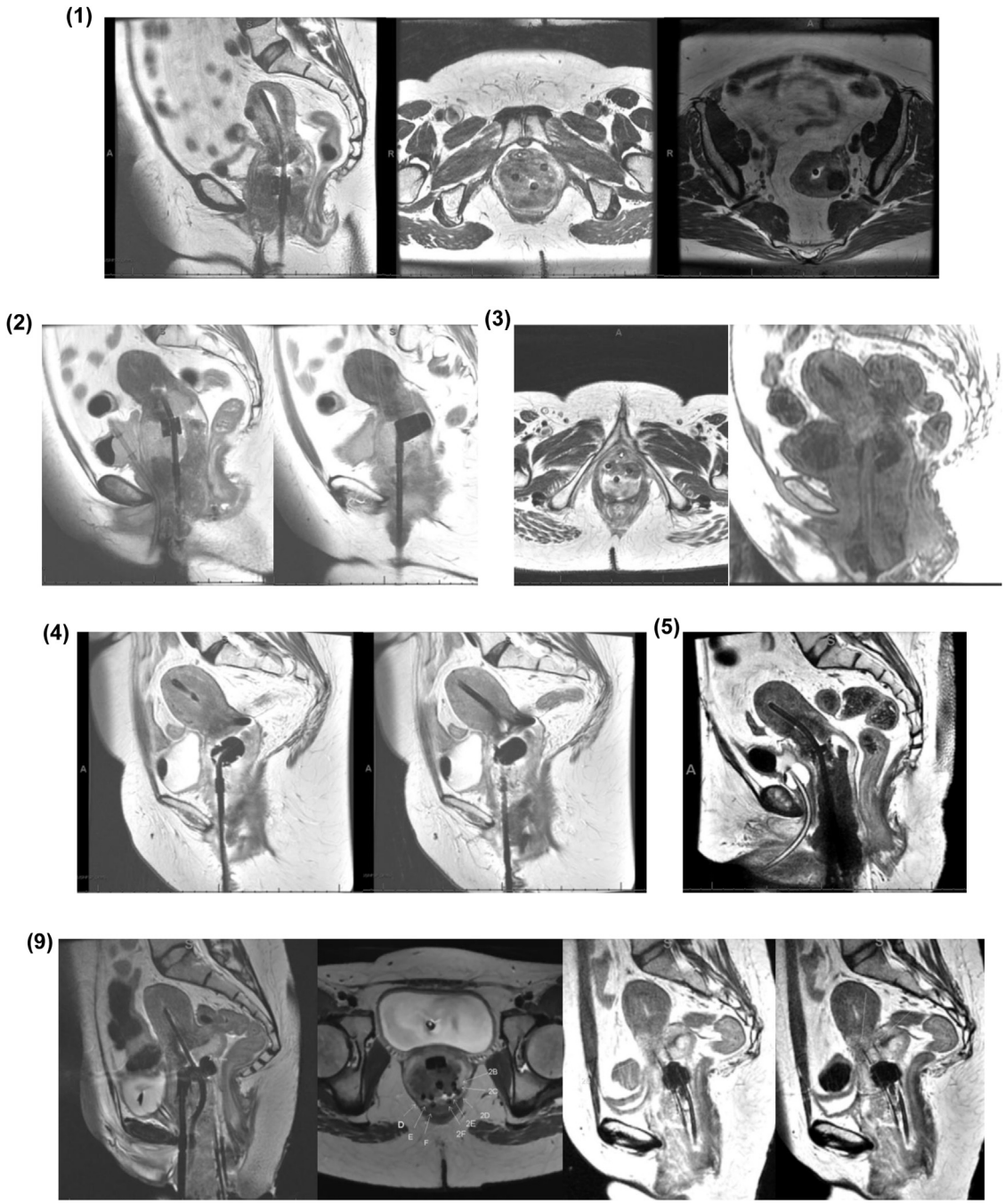

Fig. 3. Example T2-weighted MRI images demonstrating visibility of the C4:S line markers within the gynecologic brachytherapy applicator tandem-and-ovoids: on 1.5-T (cases 1−3) and 3.0-T (cases 4−5, 9 [interstitial]). Labeled by case number. White arrows label interstitial catheter positions for case 9.

Discussion

This study evaluates the clinical utility and value contribution of a novel MRI-positive line marker for brachytherapy, thereby demonstrating that (*1*) C4:S within HDPE tubing is visible on postimplant MRI across multiple sequences, magnet strengths, and image orientations; (2) these line markers facilitate treatment planning dosimetry directly on MRI through accurate source path localization and reconstruction; and (*3*) the C4:S markers can improve the MRI-guided brachytherapy workflow and decrease provider delivery costs by eliminating the need for a redundant postimplant CT (in addition to the MRI scan).

The C4:S line markers were visible on T1-/T2-weighted images and 3D-CISS/FIESTA-C sequences but demonstrated their strongest signal on the latter. The high visibility of the markers on 3D-CISS/FIESTA-C facilitated accurate delineation of the T&O applicator lumens and source paths. These imaging protocols can be feasibly used as an adjunct to conventional T1- and T2-weighted sequences for contouring and treatment planning. By

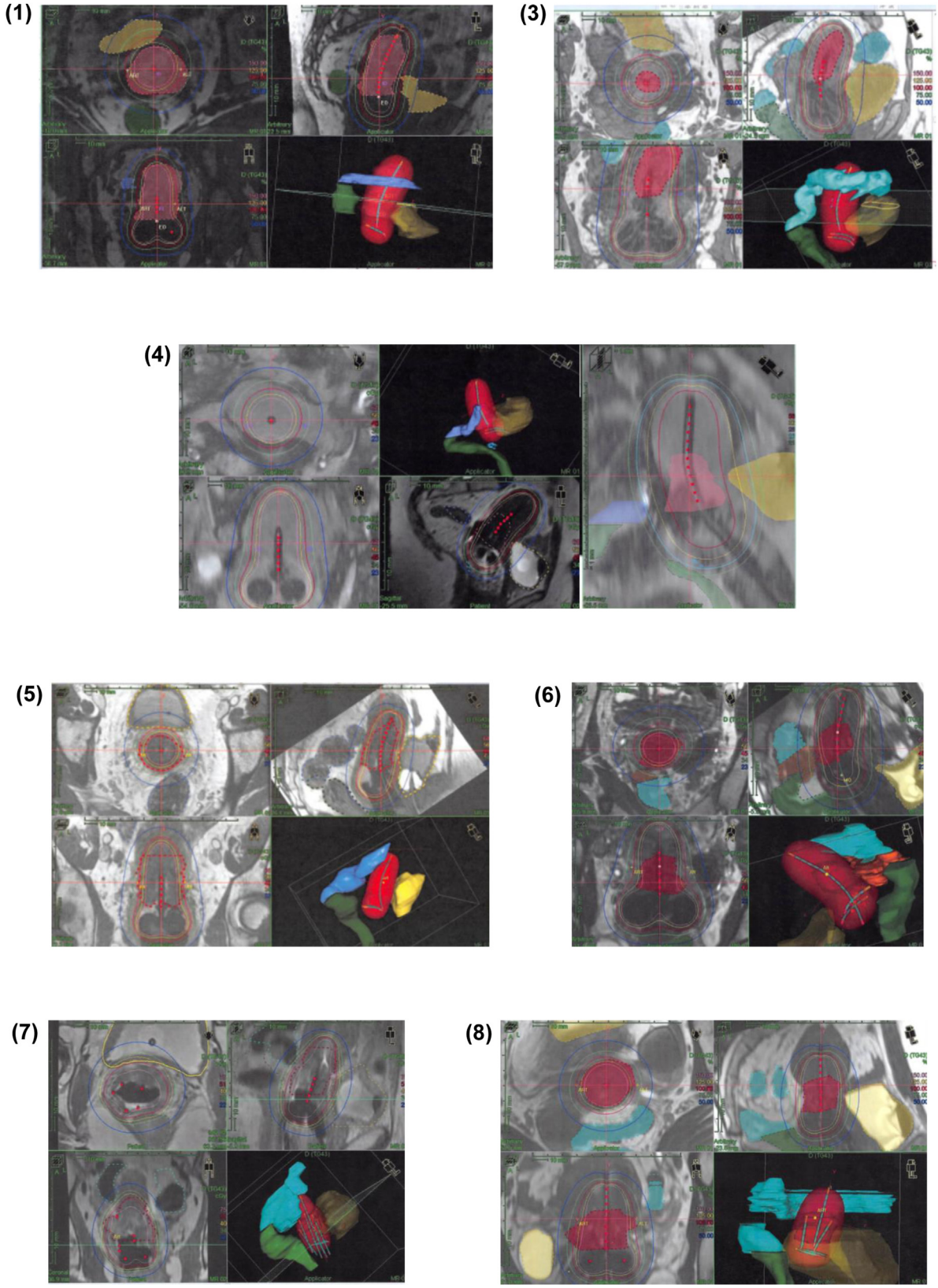

Fig. 4. Example pulsed-dose-rate (PDR) gynecologic brachytherapy treatment plans, generated directly on postimplant MRI (Oncentra planning system, Elekta, Stockholm, Sweden) with C4:S line markers inserted within the applicator tandem-and-ovoids and interstitial catheters (cases 7 and 8). Labeled by case number.

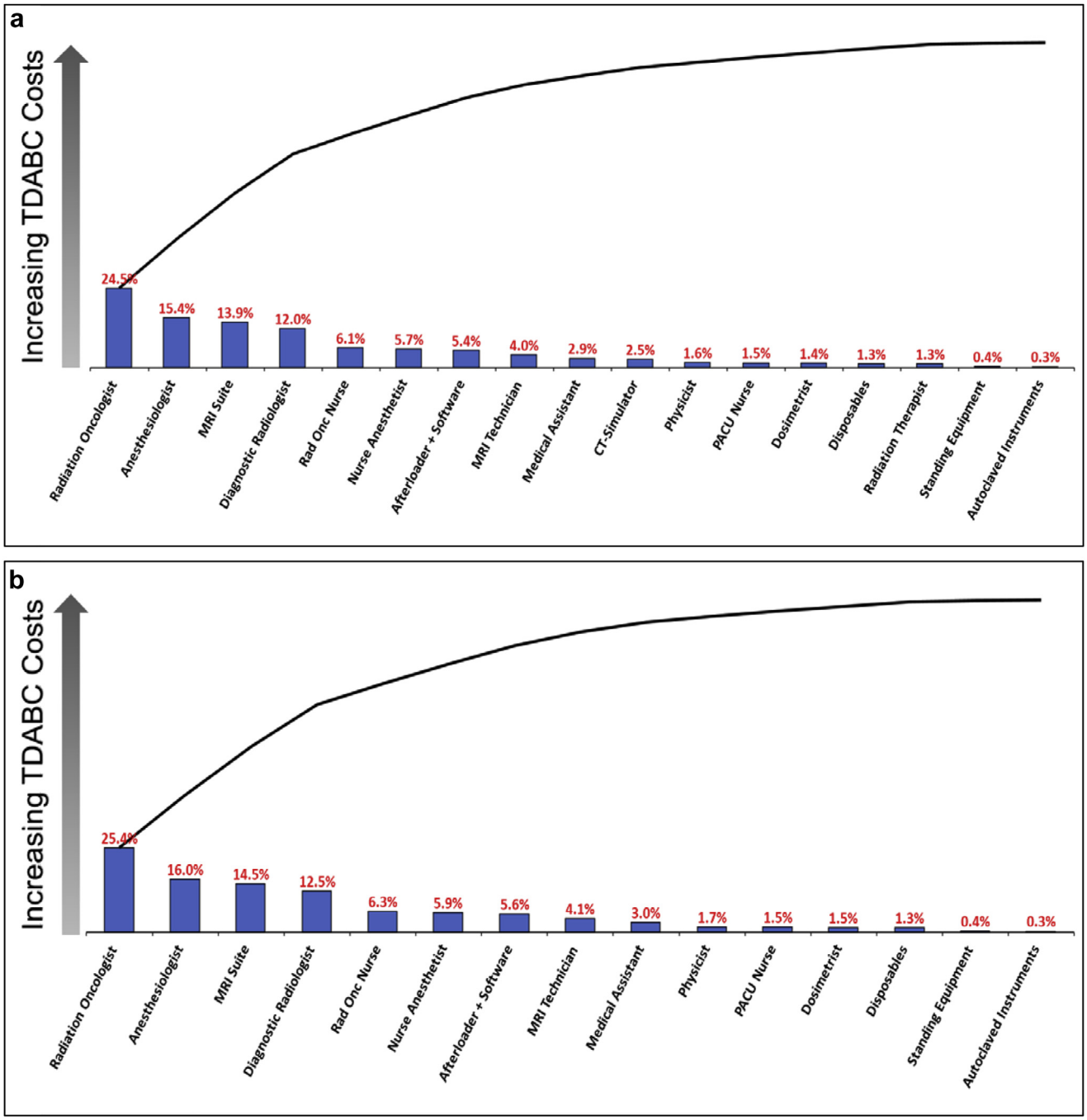

Fig. 5. (a) TDABC analysis of intraoperative MRI-guided brachytherapy over a single-implant episode, adapted from (53), with incorporation of additional 3D-CISS/FIESTA-C MRI sequences and (b) after integration of line markers into workflow. The contribution of each resource is represented as a relative portion of aggregate cost. Postoperative CT simulation, along with radiation therapist effort, account for 4% of total costs within the initial workflow (and an opportunity for resource consolidation). TDABC, time-driven activity-based costing.

uploading both image sets (obtained during the same post-implant MRI scan) into the treatment planning system, tumor delineation and dosimetric calculations can be applied directly with MRI. At present, the 3D-CISS/FIESTA-C sequences are clinically used across a range of anatomical sites (abdominal, CNS, pelvic, retroperitoneal), indications (diagnostic and interventional), and manufacturers (GE and Siemens), ensuring access and availability for other treatment centers (45–48). In addition, the visibility of C4:S was maintained for different image orientations and magnet strengths, further supporting widespread utility of the MRI-positive line markers.

Most significantly, by permitting delineation of the applicator lumen and source path directly on MRI, the C4:S line markers eliminate the need for a redundant post-implant CT scan for fusion and manual reconstruction. As

the health care industry shifts toward value-based care, the increasing costs of technological advancements should be evaluated within the setting of health care value (defined as outcomes over costs) (49,53−57). TDABC has been applied to transparently quantify the costs of brachytherapy treatment delivery from the provider standpoint (bottom-up perspective) (49−53,58−60). Here we applied TDABC to evaluate our intraoperative MRI-guided brachytherapy workflow and identify potential opportunities for internal cost savings through resource consolidation. By eliminating the redundant postimplant CT for manual reconstruction (53), the MRI-positive C4:S line markers can improve process speed while decreasing provider resource utilization associated with care delivery. Ongoing efforts to optimize marker signal on T2 sequences alone will eliminate the additional table time associated with 3D-CISS/FIESTA-C acquisition and further improve treatment delivery costs.

There are several limitations associated with this report. Although C4:S should retain MRI-positive signal through plastic interstitial catheters, platinum or titanium catheters may compromise visibility. The use of a C4-based marker-flange has been suggested for titanium applicators, with high signal and minimal inaccuracies (<2-mm) on T1-weighted images (30). Alternatively for small plastic or metal interstitial catheters, applicator modeling software may be an attractive option for direct reconstruction on MRI (20,39,61,62). Yet while vendor-supplied applicator models are available for ''standard'' applicators, a significant fraction of our cases involve custom-designed applicators which require considerable user intervention and time to ensure accuracy, rendering them a less feasible alternative than manual identification of dwell positions; therefore, applicator modeling was not available for direct TDABC comparison. In addition, our workflow requires postoperative CT simulation in a different location also used for simulation of external beam patients. Given the dual utility of these CT simulators and the additional steps and time associated with patient transport, our postoperative simulations easily contribute 60 min to the total workflow (with associated costs); however, we realize that CT simulation may require less time within a dedicated HDR CT suite at other institutions. Furthermore, our TDABC analysis did not include cost of the C4:S markers, which themselves would be associated with some market or wholesale expense to the provider, although these may be offset by additional reimbursement associated with their utilization.

In summary, we have successfully demonstrated feasibility of the C4:S line markers for MRI-guided brachytherapy. By facilitating clear delineation of the applicator lumen and source path on MRI, these novel MRI-positive markers permit accurate and precise dosimetry applicable to HDR or pulsed-dose-rate brachytherapy. Research efforts to improve T2-weighted signal are ongoing and will further expand their utility; however, the C4:S markers currently represent a practical and highly useful tool to optimize MRI-guided brachytherapy for multiple malignancies.

Acknowledgments

The authors are grateful to Andrew Bright, Anne Fisher, Steven Frank, Stacy Hash, Michelle Underwood, and Brandy Willis, for their contributions to this work.

References

[1] Han K, Milosevic M, Fyles A, *et al*. Trends in the utilization of brachytherapy in cervical cancer in the United States. *Int J Radiat Oncol Biol Phys* 2013;87:111−119.

[2] Watanabe Y, Muraishi H, Takei H, *et al*. Automated source tracking with a pinhole imaging system during high-dose-rate brachytherapy treatment. *Phys Med Biol* 2018;63:145002.

[3] Beld E, Seevinck PR, Schuurman J, *et al*. Development and testing of a magnetic resonance (MR) conditional afterloader for source tracking in magnetic resonance imaging-guided high-dose-rate (HDR) brachytherapy. *Int J Radiat Oncol Biol Phys* 2018;102:960−968.

[4] Poder J, Brown R, Howie A, *et al*. A risk-based approach to development of ultrasound-based high-dose-rate prostate brachytherapy quality management. *Brachytherapy* 2018;17:788−793.

[5] Thomadsen B, Lin SW, Laemmrich P, *et al*. Analysis of treatment delivery errors in brachytherapy using formal risk analysis techniques. *Int J Radiat Oncol Biol Phys* 2003;57:1492−1508.

[6] Wilkinson DA, Kolar MD. Failure modes and effects analysis applied to high-dose-rate brachytherapy treatment planning. *Brachytherapy* 2013;12:382−386.

[7] Williamson JF. Current brachytherapy quality assurance guidance: Does it meet the challenges of emerging image-guided technologies? *Int J Radiat Oncol Biol Phys* 2008;71:S18−S22.

[8] Wadi-Ramahi S, Alnajjar W, Mahmood R, *et al*. Failure modes and effects analysis in image-guided high-dose-rate brachytherapy: Quality control optimization to reduce errors in treatment volume. *Brachytherapy* 2016;15:669−678.

[9] Damato AL, Viswanathan AN. Magnetic resonance-guided gynecologic brachytherapy. *Magn Reson Imaging Clin N Am* 2015;23:633−642.

[10] Pötter R, Georg P, Dimopoulos JCA, *et al*. Clinical outcome of protocol based image (MRI) guided adaptive brachytherapy combined with 3D conformal radiotherapy with or without chemotherapy in patients with locally advanced cervical cancer. *Radiother Oncol* 2011;100:116−123.

[11] Charra-Brunaud C, Harter V, Delannes M, *et al*. Impact of 3D image-based PDR brachytherapy on outcome of patients treated for cervix carcinoma in France: Results of the French STIC prospective study. *Radiother Oncol* 2012;103:305−313.

[12] Jürgenliemk-Schulz IM, Lang S, Tanderup K, *et al*. Variation of treatment planning parameters (D90 HR-CTV, D 2cc for OAR) for cervical cancer tandem ring brachytherapy in a multicentre setting: Comparison of standard planning and 3D image guided optimisation based on a joint protocol for dose-volume constraints. *Radiother Oncol* 2010;94:339−345.

[13] Lindegaard JC, Tanderup K, Nielsen SK, *et al*. MRI-guided 3D optimization significantly improves DVH parameters of pulsed-dose-rate brachytherapy in locally advanced cervical cancer. *Int J Radiat Oncol Biol Phys* 2008;71:756−764.

[14] Mitchell DG, Snyder B, Coakley F, *et al*. Early invasive cervical cancer: Tumor delineation by magnetic resonance imaging, computed tomography, and clinical examination, verified by pathologic results, in the ACRIN 6651/GOG 183 Intergroup Study. *J Clin Oncol* 2006;24:5687−5694.

[15] Kim SH, Choi BI, Han JK, *et al*. Preoperative staging of uterine cervical carcinoma: Comparison of CT and MRI in 99 patients. *J Comput Assist Tomogr* 1993;17:633−640.

[16] Subak LL, Hricak H, Powell CB, *et al*. Cervical carcinoma: Computed tomography and magnetic resonance imaging for preoperative staging. *Obstet Gynecol* 1995;86:43−50.

[17] Tanderup K, Viswanathan AN, Kirisits C, *et al*. Magnetic resonance image guided brachytherapy. *Semin Radiat Oncol* 2014;24:181−191.

[18] Owrangi AM, Prisciandaro JI, Soliman A, *et al*. Magnetic resonance imaging-guided brachytherapy for cervical cancer: Initiating a program. *J Contemp Brachytherapy* 2015;7:417−422.

[19] Harkenrider MM, Alite F, Silva SR, *et al*. Image-based brachytherapy for the treatment of cervical cancer. *Int J Radiat Oncol Biol Phys* 2015;92:921−934.

[20] Kim H, Houser CJ, Kalash R, *et al*. Workflow and efficiency in MRI-based high-dose-rate brachytherapy for cervical cancer in a high-volume brachytherapy center. *Brachytherapy* 2018;17:753−760.

[21] Haie-Meder C, Pötter R, Van Limbergen E, *et al*. Recommendations from Gynaecological (GYN) GEC-ESTRO Working Group (I): Concepts and terms in 3D image based 3D treatment planning in cervix cancer brachytherapy with emphasis on MRI assessment of GTV and CTV. *Radiother Oncol* 2005;74:235−245.

[22] Pötter R, Haie-Meder C, Van Limbergen E, *et al*. Recommendations from gynaecological (GYN) GEC ESTRO working group (II): Concepts and terms in 3D image-based treatment planning in cervix cancer brachytherapy-3D dose volume parameters and aspects of 3D image-based anatomy, radiation physics, radiobiology. *Radiother Oncol* 2006;78:67−77.

[23] Viswanathan AN, Erickson B, Gaffney DK, *et al*. Comparison and consensus guidelines for delineation of clinical target volume for CT- and MR-based brachytherapy in locally advanced cervical cancer. *Int J Radiat Oncol Biol Phys* 2014;90:320−328.

[24] Hegazy N, Pötter R, Kirisits C, *et al*. High-risk clinical target volume delineation in CT-guided cervical cancer brachytherapy: Impact of information from FIGO stage with or without systematic inclusion of 3D documentation of clinical gynecological examination. *Acta Oncol* 2013;52:1345−1352.

[25] Viswanathan AN, Dimopoulos J, Kirisits C, *et al*. Computed tomography versus magnetic resonance imaging-based contouring in cervical cancer brachytherapy: Results of a prospective trial and preliminary guidelines for standardized contours. *Int J Radiat Oncol Biol Phys* 2007;68:491−498.

[26] De Brabandere M, Hoskin P, Haustermans K, *et al*. Prostate postimplant dosimetry: Interobserver variability in seed localisation, contouring and fusion. *Radiother Oncol* 2012;104:192−198.

[27] Beld E, Moerland MA, Zijlstra F, *et al*. MR-based source localization for MR-guided HDR brachytherapy. *Phys Med Biol* 2018;63:085002.

[28] Skowronek J. Current status of brachytherapy in cancer treatment - short overview. *J Contemp Brachytherapy* 2017;9:581−589.

[29] Hellebust TP, Kirisits C, Berger D, *et al*. Recommendations from Gynaecological (GYN) GEC-ESTRO Working Group: Considerations and pitfalls in commissioning and applicator reconstruction in 3D image-based treatment planning of cervix cancer brachytherapy. *Radiother Oncol* 2010;96:153−160.

[30] Schindel J, Muruganandham M, Pigge FC, *et al*. Magnetic resonance imaging (MRI) markers for MRI-guided high-dose-rate brachytherapy: Novel marker-flange for cervical cancer and marker catheters for prostate cancer. *Int J Radiat Oncol Biol Phys* 2013;86:387−393.

[31] Viswanathan AN, Szymonifka J, Tempany-Afdhal CM, *et al*. A prospective trial of real-time magnetic resonance-guided catheter placement in interstitial gynecologic brachytherapy. *Brachytherapy* 2013;12:240−247.

[32] Kamran SC, Manuel MM, Cho LP, *et al*. Comparison of outcomes for MR-guided versus CT-guided high-dose-rate interstitial brachytherapy in women with locally advanced carcinoma of the cervix. *Gynecol Oncol* 2017;145:284−290.

[33] Otter S, Coates A, Franklin A, *et al*. Improving dose delivery by adding interstitial catheters to fixed geometry applicators in high-dose-rate brachytherapy for cervical cancer. *Brachytherapy* 2018;17:580−586.

[34] Hellebust TP. Place of modern imaging in brachytherapy planning. *Cancer Radiother* 2018;22:326−333.

[35] Petric P, Kirisits C. Potential role of TRAns Cervical Endosonography (TRACE) in brachytherapy of cervical cancer: Proof of concept. *J Contemp Brachytherapy* 2016;8:215−220.

[36] De Brabandere M, Al-Qaisieh B, De Wever L, *et al*. CT- and MRI-based seed localization in postimplant evaluation after prostate brachytherapy. *Brachytherapy* 2013;12:580−588.

[37] Tanderup K, Hellebust TP, Lang S, *et al*. Consequences of random and systematic reconstruction uncertainties in 3D image based brachytherapy in cervical cancer. *Radiother Oncol* 2008;89:156−163.

[38] Frank SJ, Stafford RJ, Bankson JA, *et al*. A novel MRI marker for prostate brachytherapy. *Int J Radiat Oncol Biol Phys* 2008;71:5−8.

[39] Haack S, Nielsen SK, Lindegaard JC, *et al*. Applicator reconstruction in MRI 3D image-based dose planning of brachytherapy for cervical cancer. *Radiother Oncol* 2009;91:187−193.

[40] Perez-Calatayud J, Kuipers F, Ballester F, *et al*. Exclusive MRI-based tandem and colpostats reconstruction in gynaecological brachytherapy treatment planning. *Radiother Oncol* 2009;91:181−186.

[41] Maenhout M, van der Voort van Zyp JRN, Borot de Battisti M, *et al*. The effect of catheter displacement and anatomical variations on the dose distribution in MRI-guided focal HDR brachytherapy for prostate cancer. *Brachytherapy* 2018;17:68−77.

[42] Kataoka M, Kido A, Koyama T, *et al*. MRI of the female pelvis at 3T compared to 1.5T: Evaluation on high-resolution T2-weighted and HASTE images. *J Magn Reson Imaging* 2007;25:527−534.

[43] Hussain SM, van den Bos IC, Oliveto JM, *et al*. MR imaging of the female pelvis at 3T. *Magn Reson Imaging Clin N Am* 2006;14:537−544. vii.

[44] Besta R, Shankar YU, Kumar A, *et al*. MRI 3D CISS- A novel imaging modality in diagnosing trigeminal neuralgia - a review. *J Clin Diagn Res* 2016;10:ZE01−ZE03.

[45] Buch K, Caruso P, Ebb D, *et al*. Balanced steady-state free precession sequence (CISS/FIESTA/3D driven equilibrium radiofrequency reset pulse) increases the diagnostic yield for spinal drop metastases in children with brain tumors. *AJNR Am J Neuroradiol* 2018;39:1355−1361.

[46] Hingwala D, Chatterjee S, Kesavadas C, *et al*. Applications of 3D CISS sequence for problem solving in neuroimaging. *Indian J Radiol Imaging* 2011;21:90−97.

[47] Chavhan GB, Babyn PS, Jankharia BG, *et al*. Steady-state MR imaging sequences: Physics, classification, and clinical applications. *Radiographics* 2008;28:1147−1160.

[48] Bhosale P, Ma J, Choi H. Utility of the FIESTA pulse sequence in body oncologic imaging: Review. *AJR Am J Roentgenol* 2009;192:S83−S93. (Quiz S94-97).

[49] Ning MS, Klopp AH, Jhingran A, *et al*. Quantifying institutional resource utilization of adjuvant brachytherapy and intensity-modulated radiation therapy for endometrial cancer via time-driven activity-based costing. *Brachytherapy* 2019;18:445−452.

[50] Dutta SW, Bauer-Nilsen K, Sanders JC, *et al*. Time-driven activity-based cost comparison of prostate cancer brachytherapy and intensity-modulated radiation therapy. *Brachytherapy* 2018;17:556−563.

[51] Thaker NG, Pugh TJ, Mahmood U, *et al*. Defining the value framework for prostate brachytherapy using patient-centered outcome metrics and time-driven activity-based costing. *Brachytherapy* 2016;15:274−282.

[52] Ilg AM, Laviana AA, Kamrava M, *et al*. Time-driven activity-based costing of low-dose-rate and high-dose-rate brachytherapy for low-risk prostate cancer. *Brachytherapy* 2016;15:760−767.

[53] Ning MS, Venkatesan AM, Stafford RJ, *et al*. Developing an intraoperative 3T MRI-guided brachytherapy program within a diagnostic imaging suite: Methods, process workflow, and value-based analysis. *Brachytherapy* 2019; https://doi.org/10.1016/j.brachy.2019.09.010.

[54] Porter ME. What is value in health care? *N Engl J Med* 2010;363:2477−2481.

[55] Porter ME. Value-based health care delivery. *Ann Surg* 2008;248:503−509.

[56] Thaker NG, Ali TN, Porter ME, *et al*. Communicating value in health care using radar charts: A case study of prostate cancer. *J Oncol Pract* 2016;12:813−820.

[57] Thaker NG, Orio PF, Potters L. Defining the value of magnetic resonance imaging in prostate brachytherapy using time-driven activity-based costing. *Brachytherapy* 2017;16:665−671.

[58] Laviana AA, Ilg AM, Veruttipong D, *et al*. Utilizing time-driven activity-based costing to understand the short- and long-term costs of treating localized, low-risk prostate cancer. *Cancer* 2016;122:447−455.

[59] Bauer-Nilsen K, Hill C, Trifiletti DM, *et al*. Evaluation of delivery costs for external beam radiation therapy and brachytherapy for locally advanced cervical cancer using time-driven activity-based costing. *Int J Radiat Oncol Biol Phys* 2018;100:88−94.

[60] Thaker NG, Frank SJ, Feeley TW. Comparative costs of advanced proton and photon radiation therapies: Lessons from time-driven activity-based costing in head and neck cancer. *J Comp Eff Res* 2015;4:297−301.

[61] Berger D, Dimopoulos J, Pötter R, *et al*. Direct reconstruction of the Vienna applicator on MR images. *Radiother Oncol* 2009;93:347−351.

[62] De Leeuw AAC, Moerland MA, Nomden C, *et al*. Applicator reconstruction and applicator shifts in 3D MR-based PDR brachytherapy of cervical cancer. *Radiother Oncol* 2009;93:341−346.